Co., Ltd., an uranium fuel processing plant in Tokai-mura, Ibaraki, Japan, on 30 September 1999.[6] He was transferred from the National Institute of Radiological Sciences to the University of Tokyo Hospital on day 2. After his admission at our hospital, continuous intravenous administration of L-alanyl-L-glutamine was started expecting promotion of the epithelial regeneration of the gastrointestinal tract after radiation exposure. He received peripheral blood stem cell transplantation on days 6 and 7. Endotracheal intubation under sedation was introduced on day 10 because of gradual worsening in the patient's respiratory status and in preparation for the future deterioration in the patient's general condition. Despite the intensive care for his symptoms, exudation from the skin and diarrhea had got worse day by day. He had died on day 82. Details of the clinical course were documented previously.[7]

Daily volumes of fluid discharge are shown in Fig. 1. Clinical course related to gastrointestinal injuries is summarized below. Mild diarrhea was observed for the first two days after the accident as a symptom of prodromal syndrome and, on day 26, severe diarrhea with bilious watery stool started as a symptom of radiation-induced gastrointestinal syndrome. The volume of watery stool increased to 3500 mL per day on day 39. Bloody stool was observed starting on day 45. The volume of bloody stool increased day by day. Continuous arterial infusion of vasopressin was started from

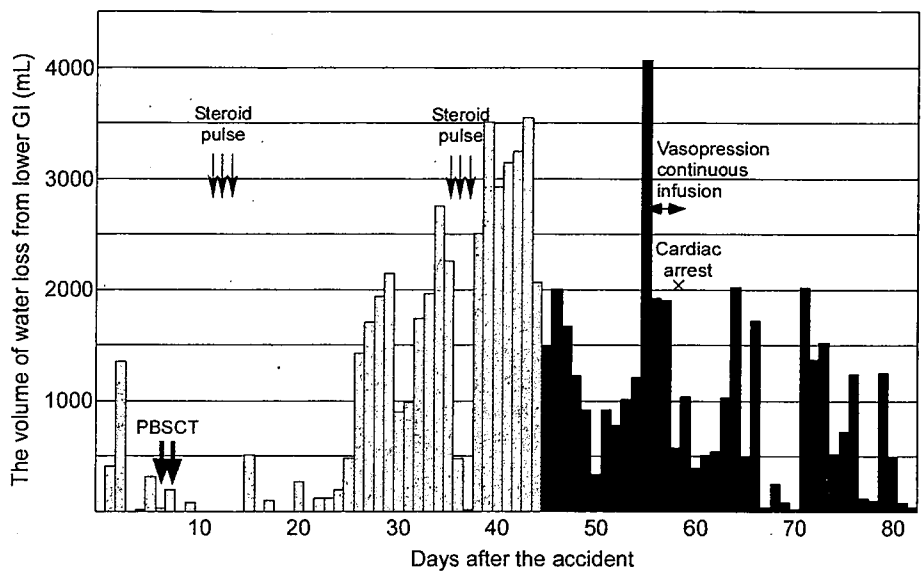

Fig. 1. Daily change in the volume of fluid loss from lower gastrointestinal tract. Light gray bars represent watery diarrhea. Bloody stool, shown by dark gray bars, started on day 45. Major treatments and events are indicated. Abbreviation: PBSCT = peripheral blood stem cell transplantation.

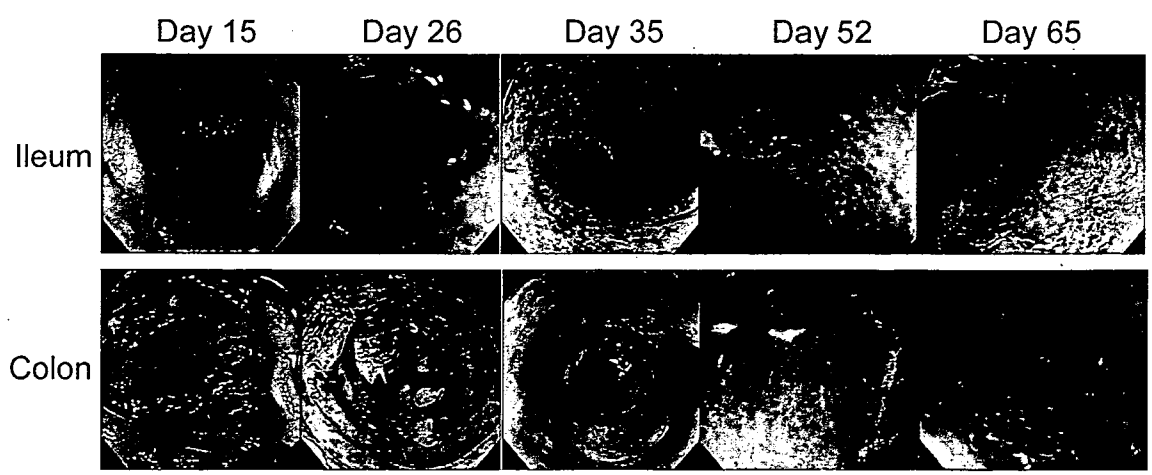

Fig. 2. The appearance of the ileum and colon by colonoscopy. The mucosa appeared almost normal on day 15, but the spots were observed on day 26. After day 35, no mucosa was observed in either the ileum or the colon. The number of bleeding sites thereafter increased.

an indwelling catheter in the superior mesenteric artery on day 55. The volume of bloody stool decreased from 4000 mL to 2000 mL per day by continuous vasopressin infusion. Vasopressin infusion, however, was discontinued on day 58, when there was a cardiac arrest of undetermined etiology. The patient was successfully resuscitated at that time. The volume of melena suddenly decreased on day 67, implying a blood clot-induced intestinal obstruction. A series of high-pressure enemas was tried thereafter but failed to relieve the obstruction. After the episode of cardiac arrest, multiple organ hypoperfusion developed, and finally the patient died of MOF on day 82.

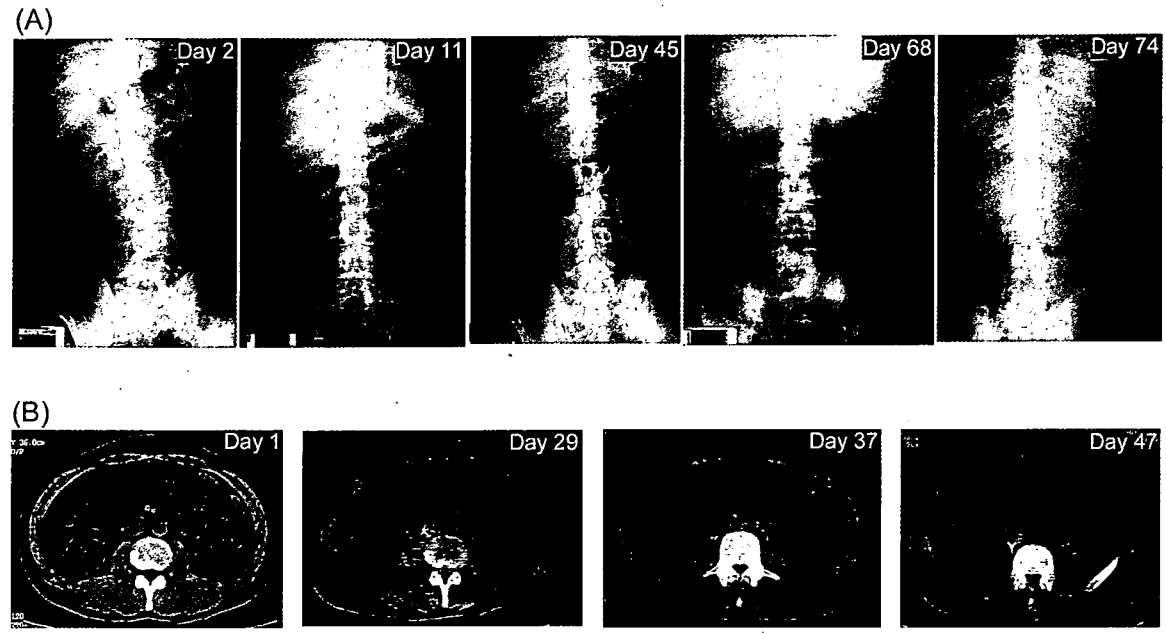

Fig. 3. Abdominal radiographs (A) and abdominal CT images (B). (A) The radiograph on day 2 appeared almost normal. Ileac gas was prominent on day 11, but Kerckring's folds were observed. On day 45, the small intestine was swollen without Kerckring's folds. The abdominal opacity decreased and the small intestine was more swollen with intestinal gas on day 68, when melena suddenly stopped. The decreased opacity of the abdomen represented the increased ascites and intestinal bleeding. On day 74, the decrease in the abdominal opacity was more prominent, and the ileac gas decreased. (B) Only the wall of the ascending colon was thickened, but the small intestine and the transverse and descending colon appeared normal on day 1. Thickening of the entire intestinal wall with the contents of fluids and air was observed on day 29. The wall thickening and the fluid collection were more prominent on day 37. The arrowhead indicates thickening of the colon wall and mesentery with intestinal fluid collection. Ascites appeared on day 47. The intestinal wall thickening was generally decreased, but the wall of the ascending colon remained thickened.

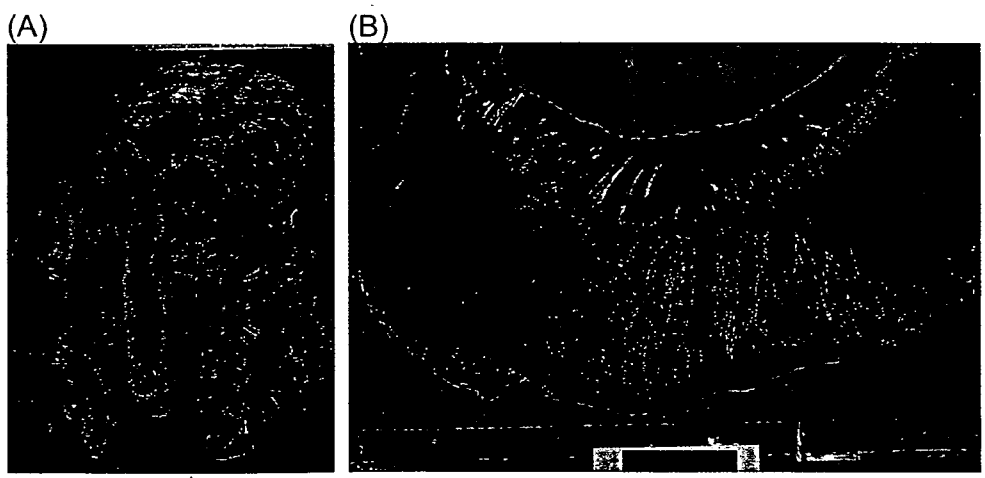

Fig. 4. The macroscopic findings at autopsy. (A) The macroscopic appearance of the small intestine and the colon, which was swollen and contained a large number of blood clots *in situ*. Erosive lesions were observed in the mucosa of the entire intestine. (B) Magnified view of the ileum. Segmental intestinal bleeding is present.

RESULTS

Endoscopic findings

Figure 2 illustrates representative serial endoscopic findings in the ileum and colon from days 15 to 65. The patient had his first colonoscopy on day 15, revealing bilious intestinal contents with no signs of mucosal injection or loss. The second colonoscopy was performed on day 26, since the volume of watery stool increased suddenly to 1433 mL a day. There were brown spottings on the sigmoid and descending colon, and the surface was covered with a pseudomembranous white coat on the transverse and ascending colon. The mucosa was generally injected, but the edematous appearance was slightly relieved compared with the findings of the previous colonoscopy. The ileal mucosa was totally lost and presented a so-called lead-pipe appearance on day 35. Colonoscopy performed on day 52 revealed that the ileal mucosal spots had increased in number. On day 65, the colon contained a large number of blood clots, which occupied the majority of the intraluminal space of the colon. Areas of patchy bleeding were observed on the ileal wall.

Radiological findings

Representative abdominal radiographs and CT images were shown in Fig. 3. CT images revealed that the wall of

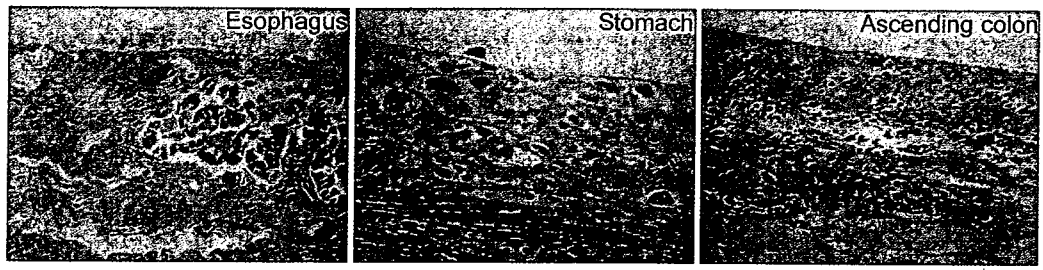

Fig. 5. Microscopic findings of the mucosa of esophagus, stomach, and ascending colon, by hematoxylin and eosin staining. In the esophagus, few squamous cells were observed and the esophageal glands were partly remnant. But, no epithelial cells were remnant in the mucosa of the stomach or ascending colon.

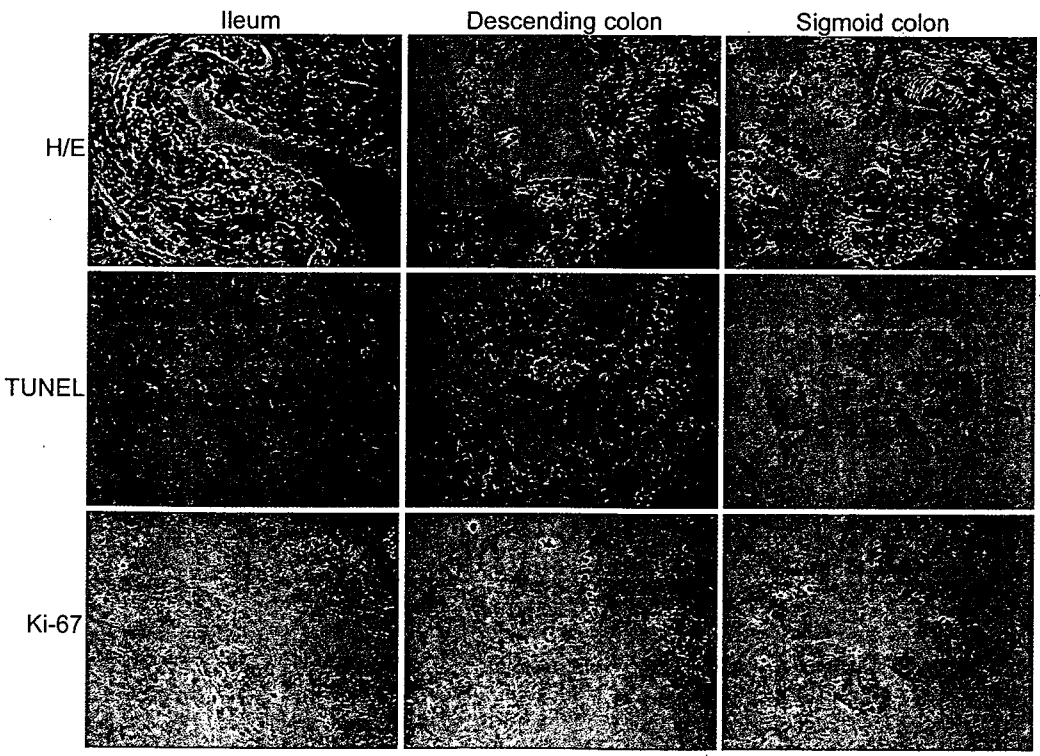

Fig. 6. Hematoxylin and eosin staining, TdT-mediated dUTP-biotin nick end labeling (TUNEL), and anti-Ki-67 immunostaining of the ileum, descending colon, and sigmoid colon. The cells positive for TUNEL, representing apoptotic cells, were hardly seen in the ileum, descending colon, or sigmoid colon. Anti-Ki-67 immunostaining revealed that there were no mitotic cells in the ileum, but 71% and 35% of the epithelial cells were positive for Ki-67 antigen in the descending and sigmoid colon, respectively.

the ascending colon was swollen and edematous as early as day 1, but there were no specific findings in other sites of the gastrointestinal tract (Fig. 3). An abdominal radiograph on day 2 was almost normal. On day 11, the dilated small bowel with prominent ileac gas was observed. The wall thickening of the entire gastrointestinal tract increased thereafter, suggesting the presence of inflammation such as infectious enteritis and radiation-induced enteritis. The volume of ascites was estimated to be 2500 mL by abdominal ultrasonography on day 42. The ileum was partly dilated with gas on day 45 on the abdominal radiograph. The attenuation level was increased in the whole abdomen, which suggested an increased volume of ascites. On day 68, dilatation of the ileum filled with gas was more remarkable. But on day 74, bowel gas decreased and the attenuation level was more prominent in the whole abdomen, which was a so-called gasless abdomen.

Postmortem examination findings

Postmortem examination was performed 4 hours after the patient's death. The stomach, jejunum, and ileum were filled with coagulated bloody content and were prominently congested at autopsy (Fig. 4). The stomach and small intestine contained 2040 g and 2680 g of clots, respectively. Throughout the gastrointestinal tract, the mucosal epithelial cells were ablated, mucosal congestion was seen, and bleeding occurred in many places (Fig. 4). Dyskaryotic cells proliferated in the stroma, and fibrotic changes in the submucosa and smooth muscle degeneration were also observed (Fig. 5 and 6).

A few squamous cells were observed in the esophagus, and the esophageal glands were partly remnant. No epithelial cells were remnant from the stomach to the ascending colon, but a few epithelial cells were observed in the descending colon, sigmoid colon, and rectum (Fig. 5 and 6). In the colon, fibrotic change was seen in the lamina propria, which was covered partially with regenerating epithelial cells. The proliferative status of the epithelial cells in the descending and sigmoid colon were examined by anti-Ki-67 immunostaining (Fig. 6). In the descending and sigmoid colon, 71% and 35% of the epithelial cells were positive for Ki-67 immunostaining, respectively. In addition, the activity of the apoptotic cascade in these epithelia was also examined by TdT-mediated dUTP-biotin nick end labeling (TUNEL) and anti-p53 and anti-p21 immunostaining (Figs. 6 and 7B). Apoptotic cells were not observed in these epi-

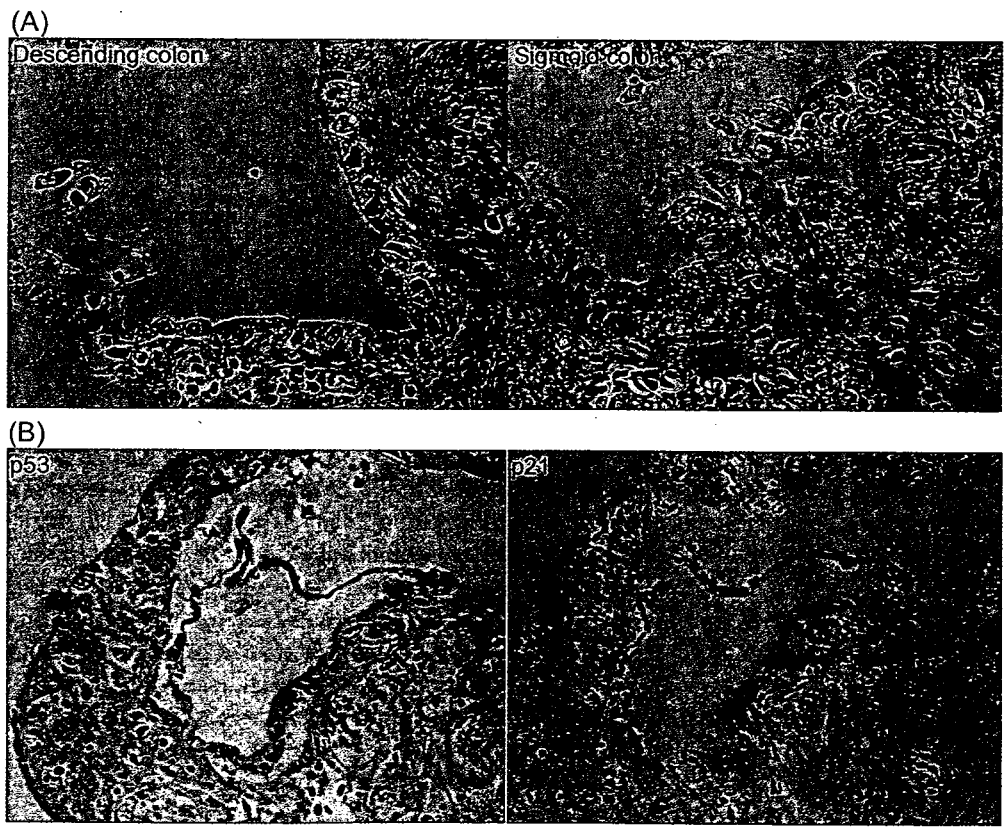

Fig. 7. (A) Magnified view of hematoxylin and eosin staining of the descending and sigmoid colon. Dyskaryosis was more severe in the descending colon than in the sigmoid colon. (B) Anti-p53 and anti-p21 immunostaining of the descending colon. Staining of the epithelial cells was negative for both.

Table 1. The estimated absorbed dose by the gastrointestinal tract

Site	Gamma ray (Gy)	Neutron beam (Gy)	Total dose (Gy)	Equivalent dose[a] (GyEq)
Esophagus	8.8–13.9	1.1– 4.6	9.8–18.5	10.6–21.7
Stomach	9.1–25.1	1.9–16.3	11.0–41.3	12.3–52.7
Small intestine	7.2–29.2	2.1–19.0	9.3–48.2	10.7–61.6
Ascending colon	20.9–33.8	15.1–24.5	36.0–58.4	46.6–75.5
Descending colon	8.4–13.7	1.0– 7.6	9.5–21.2	10.2–26.5
Sigmoid colon	10.3–12.5	3.3– 6.7	13.7–19.2	16.0–24.0

Notes. The absorbed dose of each segment of the gastrointestinal tract was estimated by projecting CT images acquired after the patient's hospitalization on the phantom model of the dose distribution.[17]
[a]The equivalent doses were calculated assuming the relative biological effectiveness of the neutron beam as 1.7 according to the report by National Institute of Radiological Sciences.[6]

thelia, because the epithelial cells were negative for TUNEL as well as for both p53 and p21 immunostaining. On the ileal mucosa, neither mitotic cells nor apoptotic cells were seen. Comparing the epithelial appearance of the descending colon and the sigmoid colon, the dyskaryosis was more severe in the epithelial cells of the former (Fig. 7A). The absorbed dose of each segment of the gastrointestinal tract was estimated from the phantom model of the dose distribution and CT images, as shown in Table 1. Although the methods of estimating these absorbed doses have uncertainties, pathological changes of the radiation-induced tissue injuries in each segment of the gastrointestinal tract appeared to be dose-dependent in general.

Major findings other than those for the gastrointestinal systems were previously reported elsewhere.[8]

DISCUSSION

We report the clinical course and the pathological features of the gastrointestinal tract in a severely radiation-exposed victim of the 1999 Tokai-mura criticality accident. At 82 days after the accident, the patient died of MOF caused by acute radiation syndrome, especially by gastrointestinal syndrome due to radiation exposure.

Abdominal radiograph revealed enlargement of the small intestine on day 11. Since then, the small intestine was consistently swollen, and Kerckring's folds were not observed on the abdominal radiograph. This suggested peristaltic dysfunction, although no clinical signs of such abnormalities were seen. The mucosa of the colon, however, appeared almost normal during the colonoscopy on day 15. These observations together indicate that functional disruption of the gastrointestinal tract preceded the morphological changes. Watery diarrhea started on day 26, and on the same day the second colonoscopy revealed multiple spotty bleeding on the mucosa of the colon. Thereafter, the symptom of watery diarrhea deteriorated and bloody diarrhea also developed. These observations can be interpreted as a collapse in the absorptive function of the gastrointestinal systems due to radiation exposure, with no obvious recovery process. Total depletion of the mucosa, which was observed both during the colonoscopy and at autopsy, appeared to cause these gastrointestinal malfunctions.

There are some previous reports on autopsy results after acute radiation exposure accidents. In the Los Alamos criticality accident of 1946[9] and in the Norwegian case of ^{60}Co gamma ray exposure in 1982,[10] victims were exposed to doses similar to that received by the patient we present here, and they died on the 9th day and 13th day after exposure, respectively (estimated approximate systemic dose of 21 Gy for the Los Alamos case and 10–30 Gy for the Norwegian case). At autopsy, the gastrointestinal epithelium was entirely depleted in those two cases.[9,10] In general, the patient experiences radiation-induced gastrointestinal syndrome 4–10 days after exposure to a dose in the range of 5–12 Gy.[11] The Los Alamos and Norwegian cases appeared to present typical clinical courses.

On the other hand, the mucosa of the colon looked almost normal in the patient we treated by the colonoscopy even on day 15. In addition, this patient did not suffer from apparent symptoms of MODS before day 18, when a deep burn developed in the right forearm and was presumed to be the onset of MODS. The reason for this difference is unknown, but the early start of intensive care for this patient might have had a good clinical effect; such care included blood stem cell transfusion on days 6 and 7, prophylactic administration of anti-bacterial, anti-fungal, and anti-viral drugs started on day 2, selective digestive tract decontamination, and intravenous administration of high-dose L-glutamine. Ziegler *et al.* suggested that infection might alter gut barrier function to facilitate translocation of bacteria and absorption of endotoxin.[12] Inflammation cascade following such major stress contributes to a patient's susceptibility to MODS.[2,4]

Many other radiation accident victims who received a systemic dose of greater than 10 Gy are reported to experience similar clinical courses of gastrointestinal malfunctions.

These symptoms included nausea, vomiting, and mild diarrhea shortly after the exposure, with no obvious deterioration for several days. Thereafter, the symptoms deteriorated progressively to watery diarrhea and bloody stool, resulting in MODS. The diminished barrier function of the gastrointestinal tract is associated with systemic infection or MOF after acute radiation exposure, as is in the case of trauma or skinburns.[3,12–15]

The systemic radiation dose was inhomogeneous. The dose to the ascending colon was assumed to be highest among segments of the gastrointestinal tract, because the patient was irradiated from the right-anterior direction from the detailed inquiry about the situations and the postures of each victims at the accident.[16–18] The severity of the radiation damage to the gastrointestinal tract in the patient presented here depended on the absorbed dose (Figs. 5 and 6 and Table 1). Total depletion of the epithelial cells in the ileum and ascending colon indicates high-dose radiation, whereas the mucosa in the esophagus, descending colon, and sigmoid colon was less damaged because of the relatively lower radiation dose. At autopsy, the epithelial cells were positive for Ki-67 staining and negative for both p51 and p21 immunostaining in the descending and sigmoid colon, implying active proliferation of the epithelial cells without activation of the apoptotic cascade (Figs. 6 and 7B). This is interpreted as the process of tissue recovery of the colon epithelium from radiation injury. Pathologically, the absorbed dose in the descending colon was speculated to be higher than that in the sigmoid colon, because the rate of Ki-67–positive epithelial cells was higher and dyskaryosis of the epithelial cells was more severe in the descending colon (Fig. 7A). These observations did not appear to reflect the estimated absorbed dose shown in Table 1 (10.7–25.2 GyE in the descending colon vs. 16.0–24.0 GyE in the sigmoid colon). Possible explanations for this include: (a) the inherent uncertainties of absorbed-dose estimation;[6,17] (b) the posture-related differences in the positions of the descending and sigmoid colon in the abdomen between the time of the accident and that of the CT examination used for calculation of the absorbed dose of each gastrointestinal segment; (c) the location on the colon of the tissue sample used for the pathological evaluations. However, pathological findings in terms of tissue injury caused by acute radiation exposure generally correlated well with the estimated absorbed dose of each segment of the gastrointestinal tract.

When a person is exposed to radiation exceeding the dose at which bone marrow death occurs, bone marrow or stem cell transplantation is generally considered.[1] For many radiation victims, however, even successful bone marrow or stem cell transplantation would not have enabled them to survive acute radiation syndrome.[7] Those patients died of MOF with severe gastrointestinal syndrome, as far as the dose was not sufficient to cause radiation-induced central nervous system or myocardial injuries. Moreover, radiation accidents themselves are rare. Accordingly, it is quite important to describe both the clinical course and the pathological confirmation and to confirm the pathology in order to assess the radiation effects on the gastrointestinal systems. In this respect, our report is unique in its focus on the clinical course and the pathological features of the gastrointestinal function.

In conclusion, the epithelial cells in the stomach, ileum, and ascending colon were totally depleted, but a small portion of the epithelial cells was remnant in the esophagus, descending colon, sigmoid colon, and rectum at autopsy. The degree of radiation injury of the gastrointestinal tract in this patient differed pathologically by the position in the abdomen, depending possibly on the radiation dose These findings we presented here in this report have not been described *in vivo* in the previous literature, although it is a well-known fact that the whole body radiation dose is inhomogeneous in the victim of an accident of high-dose radiation exposure. Detailed inquiry about the situations at the Tokai-mura criticality accident enabled us to specify the radiation dose absorbed in each segment of the gastrointestinal tract in this patient and to clarify the correlation between the absorbed dose and the severity in the gastrointestinal damages. In this point of view, detailed description of the patient's course contributes to an understanding of the fundamentals of acute radiation injuries and to clinical decision-making for the treatment of such patient.

ACKNOWLEDGMENTS

Written informed consent to publish the patient's data including descriptions, radiographs, and photographs was obtained from the patient's family.

REFERENCES

1. Browne, D., Weiss, J. F., MacVittie, T. J. and Pillai, M. V. (1992) Protocol for the treatment of radiation injuries. Adv. Space Res. **12**: 165–168.
2. Akashi, M. (2005) Role of infection and bleeding in multiple organ involvement and failure. BJR Suppl, **27**: 69–74.
3. Monti, P., Wysocki, J., van der Meeren, A. and Griffiths, N. M. (2005) The contribution of radiation-induced injury to the gastrointestinal tract in the development of multi-organ dysfunction syndrome or failure. BJR Suppl, **27**: 89–94.
4. Riedemann, N. C., Guo, R. F. and Ward, P. A. (2003) Novel strategies for the treatment of sepsis. Nat. Med. **9**: 517–524.
5. International Atomic Energy Agency. (2000) IAEA reports on Tokaimura accident. International Atomic Energy Agency. Health Phys. **78**: 231.
6. National Institute of Radiological Sciences, Final report on dose estimation for three victims of JCO accident. Ed. K. Fujimoto. NIRS, Chiba, 2002.
7. Chiba, S., Saito, A., Ogawa, S., Takeuchi, K., Kumano, K., Seo, S., Suzuki, T., Tanaka, Y., Saito, T., Izutsu, K., Yuji, K., Masuda, S., Futami, S., Nishida, M., Suzuki, G., Gale, R. P.,

Fukayama, M., Maekawa, K. and Hirai, H. (2002) Transplantation for accidental acute high-dose total body neutron- and gamma-radiation exposure. Bone. Marrow. Transplant. **29**: 935–939.
8. Uozaki, H., Fukayama, M., Nakagawa, K., Ishikawa, T., Misawa, S., Doi, M. and Maekawa, K. (2005) The pathology of multi-organ involvement: two autopsy cases from the Tokai-mura criticality accident. BJR Suppl, **27**: 13–16.
9. Goans, R. E. and Wald, N. (2005) Radiation accidents with multi-organ failure in the United States. BJR Suppl, **27**: 41–46.
10. Reitan, J. B., Brinch, L. and Beiske, K. (2005) Multi-organ failure aspects of a fatal radiation accident in Norway in 1982. BJR Suppl, **27**: 36–40.
11. Roy, L., Bertho, J. M., Souidi, M., Vozenin, M. C., Voisin, P. and Benderitter, M. (2005) Biochemical approach to prediction of multiple organ dysfunction syndrome. BJR Suppl, **27**: 146–151.
12. Ziegler, T. R., Smith, R. J., O'Dwyer, S. T., Demling, R. H. and Wilmore, D. W. (1988) Increased intestinal permeability associated with infection in burn patients. Arch. Surg. **123**: 1313–1319.
13. Goris, R. J., te Boekhorst, T. P., Nuytinck, J. K. and Gimbrere, J. S. (1985) Multiple-organ failure. Generalized autodestructive inflammation? Arch. Surg. **120**: 1109–1115.
14. Ryan, C. M., Yarmush, M. L., Burke, J. F. and Tompkins, R. G. (1992) Increased gut permeability early after burns correlates with the extent of burn injury. Crit. Care. Med. **20**: 1508–1512.
15. Baue, A. E. (1993) The role of the gut in the development of multiple organ dysfunction in cardiothoracic patients. Ann. Thorac. Surg. **55**: 822–829.
16. Ishigure, N., Endo, A., Yamaguchi, Y. and Kawachi, K. (2001) Calculation of the absorbed dose for the overexposed patients at the JCO criticality accident in Tokai-mura. J. Radiat. Res. (Tokyo), 42 Suppl: S137–148.
17. Endo, A. and Yamaguchi, Y. (2003) Analysis of dose distribution for heavily exposed workers in the first criticality accident in Japan. Radiat. Res. **159**: 535–542.
18. U. S. Environmental Protection Agency, Detailed dose assessment for the two heavily exposed workers in the Tokai-mura criticality accident. [Updated 2006 May 7; cited 2006 Nov 6]. Available from: www.epa.gov/radiation/docs/assessment/jaeri/EndoA_pres10.pdf.

Received on May 21, 2007
Revision received on July 9, 2007
Accepted on July 31, 2007
J-STAGE Advance Publication Date: October 12, 2007

J. Radiat. Res., 48, 495–503 (2007)

Regular Paper

Free Radical Scavenger Edaravone Suppresses X-ray-induced Apoptosis through p53 Inhibition in MOLT-4 Cells

Nakashi SASANO[1,2], Atsushi ENOMOTO[2], Yoshio HOSOI[2], Yosuke KATSUMURA[3], Yoshihisa MATSUMOTO[2], Kenshiro SHIRAISHI[1], Kiyoshi MIYAGAWA[2], Hiroshi IGAKI [1] and Keiichi NAKAGAWA[1]*

X-ray-induced apoptosis/Edaravone/MOLT-4 cells/Radioprotective effect/Free radical scavenger.

Edaravone, a clinical drug used widely for the treatment of acute cerebral infarction, is reported to scavenge free radicals. In the present study, we investigated the radioprotective effect of edaravone on X-ray-induced apoptosis in MOLT-4 cells. Apoptosis was determined by the dye exclusion test, Annexin V binding assay, cleavage of caspase, and DNA fragmentation. We found that edaravone significantly suppressed the X-ray-induced apoptosis. The amount of intracellular ROS production was determined by the chloromethyl-2',7'-dichlorodihydro-fluorescein diacetate system. We found that the intracellular ROS production by X-irradiation was completely suppressed by the addition of edaravone. The accumulation and phosphorylation of p53 and the expression of $p21^{WAF1}$, a target protein of p53, which were induced by X-irradiation, were also suppressed by adding edaravone. We conclude that the free radical scavenger edaravone suppresses X-ray-induced apoptosis in MOLT-4 cells by inhibiting p53.

INTRODUCTION

X-ray-induced cell death results from two types of actions, direct and indirect.[1)] In the first, the X-rays directly ionize or excite macromolecules in the cells, leading to cell damage. In the second, the X-rays excite water molecules in the cells and produce reactive oxygen species (ROS), which damage the cells. Approximately 70% of the biological damage caused by X-rays results from this indirect action.[2)] Cells that are critically damaged by X-rays will die either by interphase cell death or reproductive cell death.[3)] Most of the X-ray-induced cell deaths observed in thymocytes are of the interphase type, known as apoptosis.[4,5)] ROS are postulated to play a central role in X-ray-induced apoptosis,[6)] with the hydroxyl radical being the most important. Thus, agents that could suppress ROS would be expected to protect cells from X-ray-induced apoptosis and improve cell survival.

Edaravone (MCI-186; 3-methyl-1-phenyl-2-pyrazolin-5-one; Radicut) is a clinical drug that is used widely for the treatment of acute cerebral infarction. Its effectiveness as a treatment for this condition has been reported in many studies, including *in vivo*,[7–20)] *in vitro*,[21,22)] and clinical settings.[23–26)] Edaravone scavenges free radicals as an electron donor[27–29)]; therefore, it seemed likely to be useful for radioprotection.

Indeed, in a previous study, Anzai and colleagues reported that the intraperitoneal administration of edaravone to mice increased the lethal dose of radiation for the animals,[30)] indicating that the drug has a radioprotective effect. In that report, edaravone's radioprotective effect was probably due mainly to the suppression of bone-marrow syndrome, because the X-ray dose used in the experiment was under 10 Gy.[30)] However, edaravone's radioprotective mechanism is not fully understood at the molecular level.

Bone-marrow syndrome occurs mainly as a result of the apoptosis of stem cells.[31)] In the present study, we investigated the effect of edaravone on the apoptosis of MOLT-4 cells after X-irradiation. The human T-cell leukemia cell line MOLT-4 is highly sensitive to X-rays; after X-irradiation it undergoes an apoptotic cell death that is characterized by nuclear condensation and DNA fragmentation and is mediated by activated caspases.[32–35)] Recent studies have demonstrated that the p53 and JNK pathways are involved in the radiation-induced apoptosis of MOLT-4 cells.[34–37)] The results presented here suggest that edaravone suppresses the X-ray-induced apoptosis in MOLT-4 cells by inhibiting p53 and caspase.

*Corresponding author: Phone: +81-3-3815-5411,
Fax: +81-3-5800-8935,
E-mail: nakagawa-rad@umin.ac.jp
[1]Department of Radiology, Graduate School of Medicine, The University of Tokyo; [2]Section of Radiation Biology, Center for Disease Biology and Integrative Medicine, Faculty of Medicine, The University of Tokyo; [3]Nuclear Engineering Research Laboratory, Graduate School of Engineering, The University of Tokyo.
doi:10.1269/jrr.07061

MATERIALS AND METHODS

Cell culture

Human T-cell leukemia MOLT-4 cells were cultured in suspension with RPMI-1640 medium (Sigma) containing 5% fetal bovine serum (Hyclone) and antibiotics (100 units/ml of penicillin/streptomycin), and incubated at 37°C in a humidified atmosphere of 5% CO_2 and 95% air.

Chemicals

Edaravone was kindly provided by the Mitsubishi Pharma Corporation (Tokyo, Japan). We dissolved 52.5 mg edaravone in 192.5 μl of 2 M NaOH and 1.05 ml of DDW, and then adjusted the pH to 8.8 with 2 M HCl. Finally, physiological saline was added to adjust the final concentration of edaravone to 30 mg/ml.

X-irradiation

X-irradiation was performed with an X-ray generator (Pantak HF 350, Shimadzu) at 200 kVp and 20 mA, with a filter of 0.5 mm Cu and 1 mm Al, and at a dose rate of 1.35–1.40 Gy/min.

Dye exclusion test

One hundred microliters of cell suspension (approximately 5×10^5 cells/ml) was mixed with 25 μl of 1% erythrosin B in phosphate-buffered saline (PBS). The numbers of stained (dead) cells and unstained (live) cells were counted and the viability (%) was calculated as follows:

Viability (%) = (number of unstained cells/ total cell number) × 100

Annexin V Binding Assay

The extent of apoptosis was determined by Annexin V-FITC and propidium iodine (PI) staining, using the MEBCYTO Apoptosis Kit (MBL). Flow cytometric analysis was carried out with an EPICS flow cytometer (XL System II, Beckman Coulter), using a single laser emitting excitation light at 488 nm. In the FITC/PI diparametric plot, quadrants 1 (lower FITC/ upper PI), 2 (upper FITC/ upper PI), 3 (lower FITC/ lower PI), and 4 (upper FITC/ lower PI) represent the fractions of secondary-necrotic, primary-necrotic, viable, and apoptotic cells, respectively. More than 5,000 cells were subjected to the analysis.

Quantification of intracellular ROS

The amount of intracellular ROS production was measured by chloromethyl-2', 7'-dichlorodihydro-fluorescein diacetate (CM-H_2-DCFDA, Molecular Probes). MOLT-4 cells were incubated in the dark with approximately 5 μg/ml of probe CM-H_2-DCFDA for an hour, and the fluorescence intensity was analyzed by an EPICS flow cytometer (XL System II, Beckman Coulter) using a laser excitation and emission wavelength of 492–495 nm and 517–527 nm, respectively.

Western blot analysis

Cells were lysed in a sodium dodecyl sulfate (SDS) sample buffer (1% SDS, 3% β-mercaptoethanol, 5% glycerol, 62.5 mM, Tris-HCl, pH 6.8). Proteins were separated by 10% or 15% SDS-polyacrylamide gel electrophoresis (SDS-PAGE) and were transferred onto polyvinylidene difluoride membranes (Immobilon, Millipore). After blocking for 30

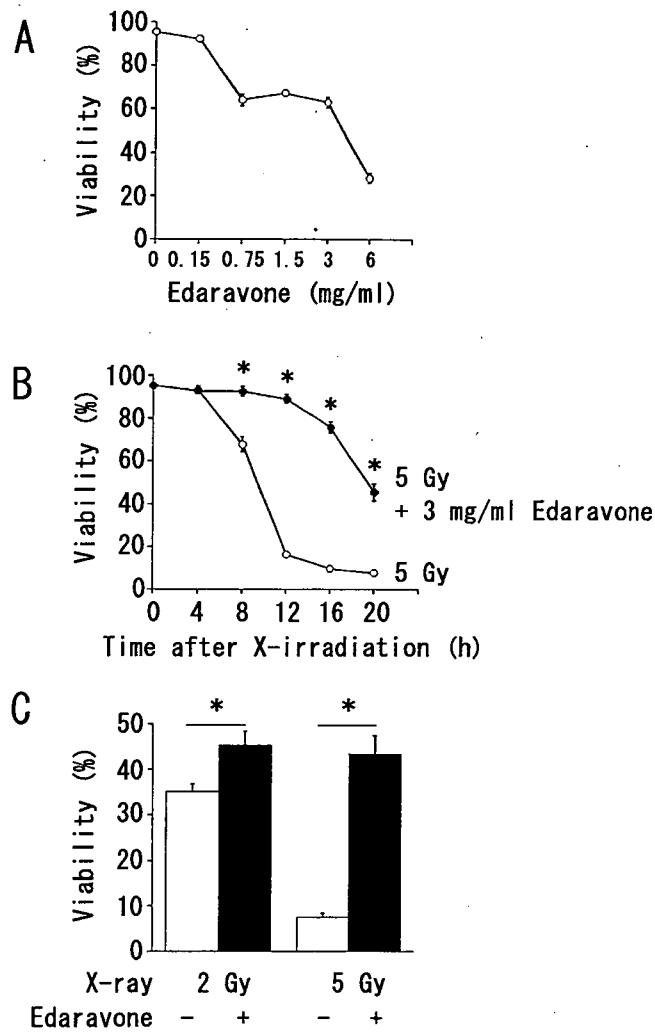

Fig. 1. Cell viabilities were determined by dye exclusion test using erythrosin B. (A) The toxicity of edaravone was examined at various concentrations. Cell viability was determined 20 hours after edaravone administration. (B) Time course of cell viability after X-irradiation. MOLT-4 cells were untreated or treated with 3 mg/ml edaravone, then subjected to 5 Gy X-irradiation 5 minutes later. (C) Effects of radiation dose on cell viability. MOLT-4 cells were irradiated at 2 or 5 Gy with or without edaravone pretreatment as in B, and the cell viability was determined 20 hours later. Data shown are means ± SD from at least three independent experiments. *$p < 0.05$.

minutes in 5% skim milk in Tris-buffered saline (TBS, 29 mM Tris-HCl, 0.9% NaCl, pH 7.6) supplemented with 0.05% Tween-20 (TBS-T), the membranes were incubated overnight at 4°C in TBS-T containing 5% skim milk and primary antibodies. The primary antibodies were anti-p53 (clone DO-1, Santa Cruz Biotechnology), anti-phospho p53 at Ser 15 (Calbiochem), anti-cleaved caspase-3 (Cell Signaling), anti-caspase-7 (MBL), anti- $p21^{WAF1}$ (Calbiochem), and anti-Bcl-2 (Pharmingen). After being rinsed with TBS-T three times, the membranes were incubated overnight at 4°C in TBS-T containing 5% skim milk and secondary antibodies conjugated with horseradish peroxidase (DAKO). The membranes were then washed three times with TBS-T, once with TBS (20 mM Tris-HCl, pH 7.5, 150 mM NaCl), and developed using an ECL-plus kit (Amersham Biosciences). The signals were obtained by exposure to X-ray

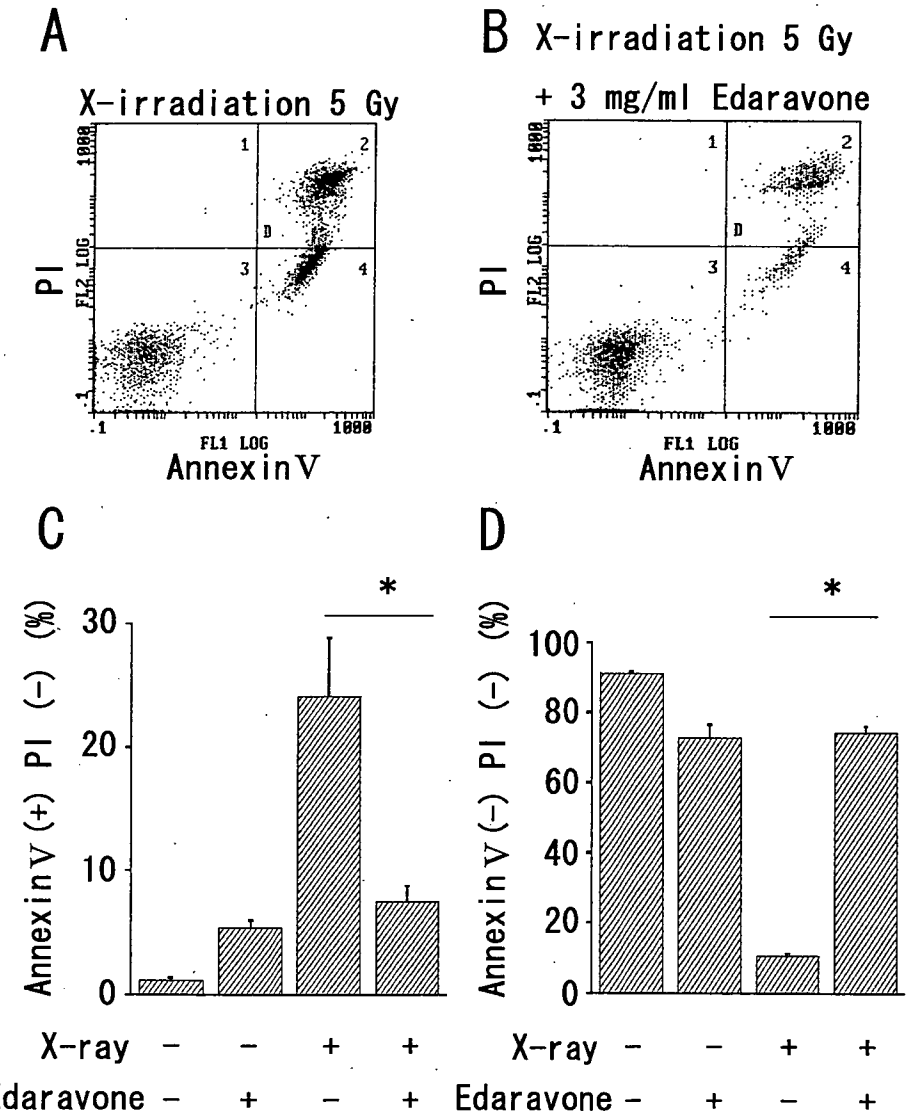

Fig. 2. Effect of edaravone on apoptosis, determined by Annexin V- PI staining. (A) MOLT-4 cells were subjected to 5 Gy X-irradiation without edaravone treatment. (B) MOLT-4 cells were subjected to 5 Gy X-irradiation 5 minutes after the addition of 3 mg/ml edaravone. Typical flow cytometry results of Annexin V- PI staining performed 16 hours after X-irradiation are shown. The transverse axis shows Annexin V -stained cells and the vertical axis shows PI-stained cells. (C) The percentage of cells stained by Annexin V and unstained by PI, which is interpreted as in the early stage of apoptosis, is shown. MOLT-4 cells were harvested 16 hours after treatment (5 Gy X-irradiation and/or 3 mg/ml edaravone 5 minutes before X-irradiation). (D) The percentage of cells unstained both by Annexin V and PI is shown. MOLT-4 cells were harvested 20 hours after treatment (5 Gy X-irradiation and/or 3 mg/ml edaravone 5 minutes before X-irradiation). *$p < 0.05$.

films (Hyperfilm MP, Amersham Biosciences).

Analysis of DNA fragmentation

Approximately 1×10^6 of control or treated cells were harvested at the indicated time points. DNA was extracted using the Apoptosis Ladder Detection Kit (WAKO), according to the manufacturer's instructions. The DNA pellet was washed, resuspended, and subjected to electrophoresis on a 1.5% agarose gel at 100 volts for 30 minutes. The gel was visualized by staining with 1 μg/ml ethidium bromide and observed under a UV transilluminator and photographed.

Statistical analysis

All experiments were repeated at least three times. The results are expressed as the mean ± standard deviation (SD) of the mean. All laboratory data were evaluated according to standard statistical methods, using commercially available computer programs such as Microsoft Excel 2000. Statistical differences were determined using the Student's *t*-test. In all tests, p values less than 0.05 were considered statistically significant.

RESULTS

Effects of edaravone on X-ray-induced cell death

First, to determine the optimal concentration of edaravone to use in the experiments, we investigated its cytotoxicity using the dye exclusion test. The cell viability was examined in cultures treated with 0.15, 0.75, 1.5, 3, and 6 mg/ml edaravone (Fig. 1A). At concentrations of edaravone less than 3 mg/ml, the cell viability was more than approximately 60%, which was considered acceptable. A dose of 6 mg/ml, however, proved cytotoxic for MOLT-4 cells (Fig. 1A). Thus, we performed the following experiments using a concentration of 3 mg/ml.

To examine the effects of edaravone on X-ray-induced cell death, we determined the time course of cell viability after 5 Gy X-irradiation with or without 3 mg/ml edaravone, using the dye exclusion test. When MOLT-4 cells were irradiated without edaravone, the cell viability 4, 8, 12, 16, and 20 hours after X-irradiation was 93.3 ± 1.7%, 67.8 ± 3.4%, 16.5 ± 1.2%, 9.6 ± 1.4%, and 7.7 ± 0.8%, respectively (Fig. 1B). When edaravone was added 5 minutes before the X-irradiation, the cell viability was 92.8 ± 1.4%, 92.6 ± 2.4%, 89.2 ± 2.0%, 75.8 ± 2.6%, and 45.6 ± 4.1%, respectively (Fig. 1B). The cell viability with edaravone was significantly higher from 8 to 20 hours after X-irradiation than that of cells that were not treated with edaravone ($p < 0.05$). These data indicate that edaravone significantly inhibited the X-ray-induced cell death of MOLT-4 cells. We also performed the same examination with 1.5 mg/ml edaravone, however, the cell viability did not increase significantly when 1.5 mg/ml edaravone was added 5 minutes before X-irradiation (data not shown).We considered that less than 1.5 mg/ml edaravone had no effect on the MOLT-4 cell viability after X-irradiation.

Next, we examined the effect of the radiation dose on the cell viability after X-irradiation. MOLT-4 cells were untreated or treated with 3 mg/ml edaravone, then subjected to 2 or 5 Gy X-irradiation 5 minutes later. The dye exclusion test was performed 20 hours after X-irradiation. The cell viability after 2 and 5 Gy X-irradiation without edaravone was 36.7 ± 1.7% and 7.7 ± 0.8%, respectively (Fig. 1C). The cell viability after 2 and 5 Gy X-irradiation with edaravone treatment was 45.5 ± 2.9% and 45.6 ± 4.1%, respectively (Fig. 1C). The cell viability at X-ray doses of 2 and 5 Gy was significantly improved by the addition of edaravone ($p < 0.05$).

Next, we examined the effect of the edaravone added after X-irradiation on the cell viability. MOLT-4 cells were subjected to 5 Gy X-irradiation, then untreated or treated with 3 mg/ml edaravone 4 hours later. The dye exclusion test was performed 20 hours after X-irradiation. The cell viability was partially improved when edaravone was added 4 hours after X-irradiation (data not shown).

Effects of edaravone on apoptosis

To assess the effect of edaravone on X-ray-induced apoptosis, we performed Annexin V-PI staining 16 or 20 hours after X-irradiation by flow cytometry. The appearance of Annexin V+/PI– cells, which were interpreted as in the early stage of apoptosis, was significantly suppressed by the addition of 3 mg/ml edaravone 5 minutes before X-irradiation ($p < 0.05$) (Fig. 2A–C). The percentage of Annexin V–/PI– cells, which were interpreted as viable, was 10.6 ± 0.8% when the cells were irradiated without 3 mg/ml edaravone

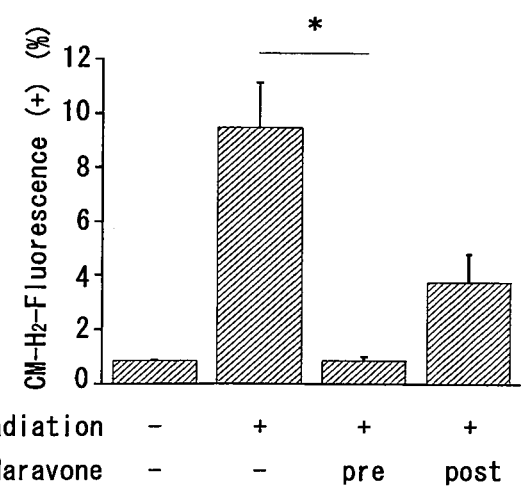

Fig. 3. Intracellular ROS determined by the CM-H_2-DCFDA flow cytometry system. The amount of intracellular ROS after treatment (20 Gy X-irradiation with or without 3 mg/ml edaravone) is shown. Edaravone was added 5 minutes before or after X-irradiation. The ROS production of each sample was quantified as described in Materials and Methods. Data shown are means + SD from at least three independent experiments. *$p < 0.05$.

and 74.2 ± 2.1% when they were X-irradiated with edaravone ($p < 0.05$) (Fig. 2D). These data indicate that the radioprotective effect of edaravone is due to the suppression of apoptosis.

We also examined the effect of 3 mg/ml edaravone added 4 hours after X-irradiation on X-ray-induced apoptosis. Annexin V-PI staining was performed 16 hours after 5 Gy-X-irradiation. The appearance of Annexin V+/PI– cells was partially suppressed by the addition of 3 mg/ml edaravone 4 hours after X-irradiation (data not shown).

Effects of edaravone on the production of intracellular ROS

To examine the effect of edaravone on the X-ray-induced production of intracellular ROS, we used the CM-H_2-DCFDA flow cytometry system.[38] CM-H_2-DCFDA is a fluorescence-based probe that was recently developed to detect the intracellular production of ROS. CM-H_2-DCFDA

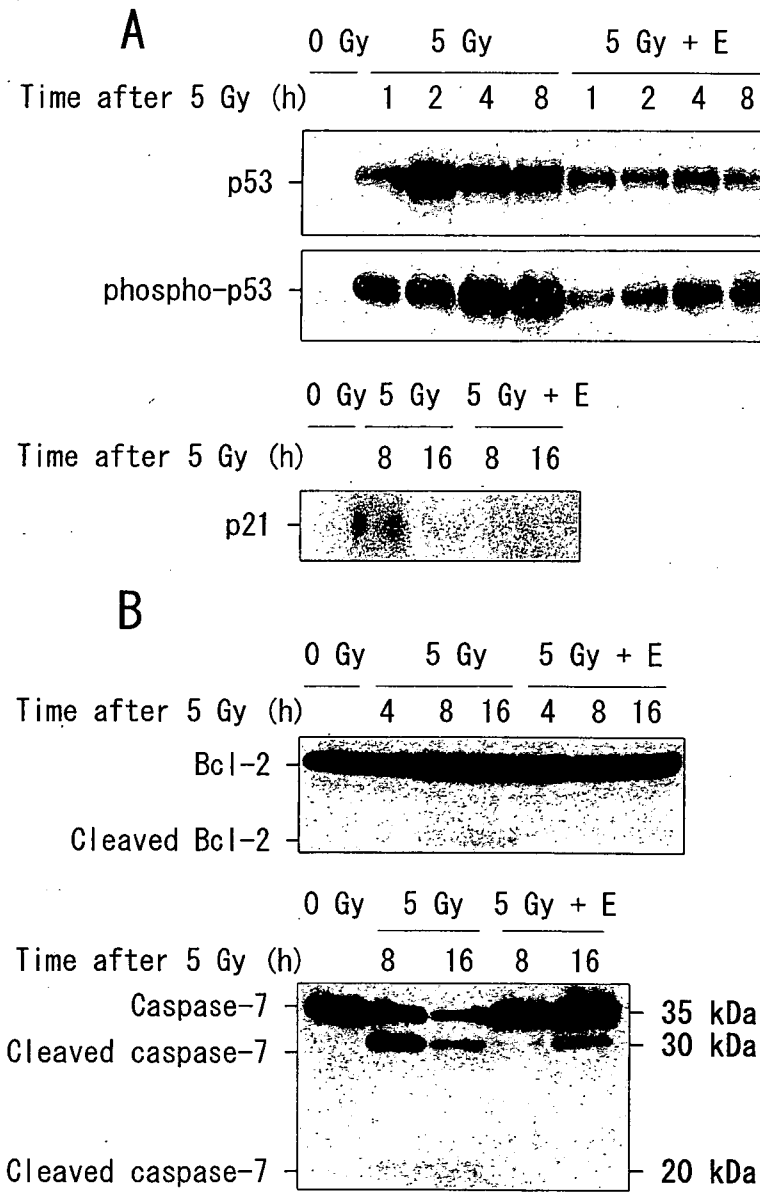

Fig. 4. Time course of the effects of edaravone (E) on apoptosis-related proteins. MOLT-4 cells were untreated or treated with 3 mg/ml edaravone, then subjected to X-irradiation at 5 Gy 5 minutes later. Proteins were detected by immunoblotting. (A) Effects of edaravone on the accumulation and phosphorylation on Ser 15 of p53 and the induction of $p21^{WAF1}$, a p53 target gene, after X-irradiation. (B) Effects of edaravone on apoptosis-related proteins Bcl-2 and caspase-7.

diffuses passively into cells, is trapped inside, and is deacetylated by intracellular esterases. It is subsequently oxidized to a fluorescent product in the presence of intracellular ROS. The oxidation of CM-H_2-DCFDA can be monitored as a convenient determinant of the level of intracellular oxidative stress. X-irradiation at 20 Gy induced an approximately 11-fold increase in basal CM-H_2-DCFDA fluorescence ($p < 0.05$), which was completely suppressed by adding 3 mg/ml edaravone 5 minutes before X-irradiation (Fig. 3). When 3 mg/ml edaravone was added 5 minutes after X-irradiation, however, the basal CM-H_2-DCFDA fluorescence did not decrease significantly (Fig. 3). These data suggest that edaravone eliminates the short-term intracellular ROS generated by X-irradiation.

Effects of edaravone on apoptosis-related proteins

We next investigated the effect of edaravone on the accumulation of p53 and on the phosphorylation of p53 at Ser 15 after X-irradiation, by immunoblotting. Fig. 4A shows that both the accumulation of p53 and its phosphorylation at Ser 15 were apparent 1 hour after X-irradiation, and both were suppressed by 3 mg/ml edaravone. Next, we investigated the expression of the p53 target gene, $p21^{WAF1}$. The expression of $p21^{WAF1}$ was apparent 8 hours after X-irradiation, and this expression was inhibited by 3 mg/ml edaravone (Fig. 4A).

We further investigated the effect of edaravone on caspase-3, caspase-7, and Bcl-2 after X-irradiation. The cleavage of caspase-3 was detectable 8 hours after X-irradiation, and this induction was almost completely suppressed by adding 3 mg/ml edaravone (data not shown). The cleavage of caspase-7 induced by X-irradiation was also suppressed by the addition of 3 mg/ml edaravone (Fig. 4B). On the other hand, Bcl-2, which is a known anti-apoptotic protein, was not overexpressed in response to edaravone addition, suggesting that Bcl-2 might not be responsible for the inhibition of apoptosis by edaravone. The cleavage of Bcl-2 was induced 16 hours after X-irradiation, and this cleavage was suppressed by edaravone addition (Fig. 4B), consistent with Bcl-2's status as a substrate molecule for caspase-3. These data indicate that the addition of edaravone before X-irradiation affects the p53 pathway and caspase activation, but not Bcl-2 overexpression.

Effects of edaravone on DNA fragmentation

DNA fragmentation is a hallmark of apoptosis.[39] It is induced by the activation of caspases, including caspase-3.[39] We examined the effect of edaravone on DNA fragmentation in MOLT-4 cells after X-irradiation. DNA fragmentation was detectable 8 hours after irradiation, and was almost completely suppressed by the addition of 3 mg/ml edaravone (Fig. 5), confirming that the activation of caspase was suppressed by edaravone. The electrophoretic pattern of DNA extracted from MOLT-4 cells irradiated with 5 Gy without addition of edaravone showed a smear pattern, not a ladder pattern, which is compatible with the observation of Akagi and colleagues.[40]

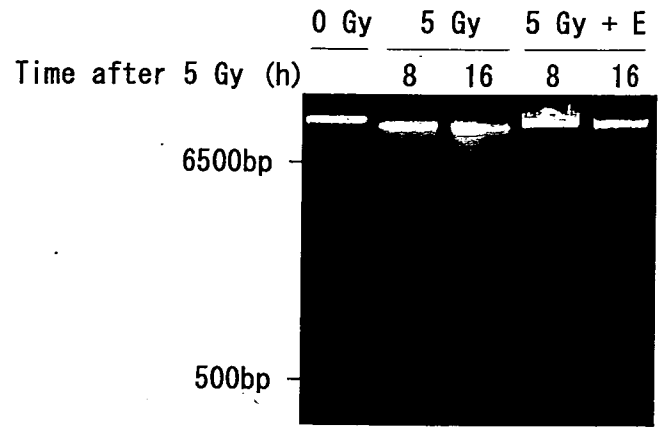

Fig. 5. Effects of edaravone (E) on the DNA fragmentation of irradiated MOLT-4 cells. Cells were untreated or treated with 3 mg/ml edaravone, then subjected to 5 Gy X-irradiation 5 minutes later. The cells were harvested 8 or 16 hours after X-irradiation and analyzed for DNA fragmentation by agarose gel electrophoresis.

DISCUSSION

We found that edaravone suppressed X-ray-induced cell death *in vitro* (Fig. 1). This finding is consistent with the results of a previous *in vivo* study, in which the lethal dose of X-irradiation for mice increased after the administration of edaravone.[30] In addition, we found that this radioprotective effect is due to the suppression of apoptosis (Fig. 2). Previous reports indicated that ROS play a crucial role in the induction of apoptosis.[41,42] We therefore investigated the amount of ROS after X-irradiation with or without edaravone addition, and found that the ROS were significantly suppressed when edaravone was added 5 minutes before X-irradiation, whereas the suppression was not significant when the drug was added 5 minutes after X-irradiation (Fig. 3). This result supports the previous finding that edaravone added after X-irradiation is ineffective as a radioprotector *in vivo*.[30] Edaravone, which exists as an anion in solution, provides an electron to ROS generated by X-irradiation and inactivates them.[27–29] One of the most important ROS is the hydroxyl radical, which reacts with biological components immediately upon being generated, and diminishes soon thereafter. Adding edaravone 5 minutes after X-irradiation might be too late to scavenge hydroxyl radicals generated by the X-irradiation, which could explain its lack of effectiveness at this time point. We propose that edaravone suppresses X-ray-induced apoptosis mainly by scavenging ROS. However, X-ray-induced apoptosis was partially suppressed even when edaravone was added 4 hours after X-irradiation. Other mechanisms may be related to the suppression of apoptosis, however, and further investigation is needed.

p53 is a transcription factor that is well-known to be involved with the cell's decision between apoptosis and other fates after X-irradiation. After DNA damage, p53's stability is increased by phosphorylation,[36] and the accumulated p53 induces the transcription of its target genes,[43] one of which is a cyclin kinase inhibitor, $p21^{WAF1}$.[44] The overexpression of a dominant-negative form of p53 in MOLT-4 cells results in a resistance of the cells to radiation-induced apoptosis.[31] We found that edaravone suppressed the X-ray-induced accumulation of p53 and its phosphorylation at Ser 15 (Fig. 4A). The expression of $p21^{WAF1}$ after X-irradiation was also suppressed by edaravone, confirming that it inhibited the X-ray-induced p53 activation (Fig. 4A).

Caspases are a family of aspartate-specific cysteine proteases that are activated during apoptosis. They are normally present in cells as proenzymes and require limited proteolysis for activation of their enzymatic activity. Activated caspases precipitate the irreversible commitment of the cell to apoptotic death by cleaving a number of substrates, one of which is Bcl-2.[45–47] Bcl-2 is an integral membrane protein that inhibits the apoptosis induced by various stimuli, including heat shock, serum depletion, and chemotherapy agents.[48] We previously reported that MOLT-4 cells transfected with mouse Bcl-2 (MOLT-4/ mbcl-2) are resistant to X-rays; that is, X-ray-induced apoptosis/rapid cell death was significantly suppressed in the Bcl-2-transfected cells.[34] It is reported that the loop domain of Bcl-2 is cleaved at Asp 34 by caspase-3 *in vitro*, and the carboxyl-terminal Bcl-2 cleavage product is pro-apoptotic.[49] In this study, the cleavage of caspase-3 and caspase-7 induced by X-irradiation was suppressed by the prior addition of edaravone (data not shown, Fig. 4B). The findings that edaravone suppresses the activation of p53 and the cleavage of caspase-3 and caspase-7 could be explained by its suppression of ROS. In contrast, the expression of Bcl-2, an anti-apoptotic protein, did not change with the addition of edaravone before X-irradiation (Fig. 4B). This observation is inconsistent with some previous reports, in which the expression of Bcl-2 was increased by edaravone in cerebral ischemic models *in vivo*[15,50] and *in vitro*.[51] The discrepancy between the present results and those of previous studies *in vivo*[15,50] might be related to differences between the *in vitro* and *in vivo* conditions. The discrepancy may also be due to differences in the genetic background of the cells used, MOLT-4 vs. PC12, and/or in the apoptotic stimuli used, X-rays vs. oxygen-glucose deprivation.[51] Another previous report suggested that the X-ray-induced apoptosis in MOLT-4 cells is fully p53-dependent.[32]

Several compounds have been shown to protect living cells from the deleterious effects of X-irradiation. The reported mechanisms of radioprotection, however, differ from compound to compound. For instance, vanadate directly suppresses p53 transactivation,[45] although its affect on ROS has not been investigated. Various antioxidants, including alpha lipoic acid or carboxycysteine-lysine salt, amifostine, reduced glutathione, and vitamin A plus vitamin E plus Vitamin C, all suppressed ROS *in vivo*.[52] Inanami and colleagues reported that a vitamin E analogue, Trolox, which is reported to inhibit lipid peroxidation,[53] suppresses the X-ray-induced apoptosis of MOLT-4 cells by inhibiting the caspase-3-dependent pathway.[54] Edaravone is also reported to inhibit lipid peroxidation,[11,19,55,56] and we found here that it suppressed p53 and caspase activation. Amifostine is a clinical drug with cytoprotective activity against the adverse effects of radiotherapy and chemotherapy in normal tissues; this cytoprotection is attributed to its radioprotective ability to scavenge free radicals[57] and to its antimutagenic effects.[58] These similar and dissimilar mechanisms of the suppression of apoptosis by various agents are still controversial.

Taking our findings together, we conclude that edaravone scavenges ROS generated by X-irradiation, which suppresses the activation of the p53- and caspase- mediated apoptotic pathway and of DNA fragmentation, and, thus, suppresses X-irradiation-induced apoptosis. Since malignant tumors often are hypoxic, edaravone might protect only normal tissues, not malignant tumors, from X-ray-induced cell damage in radiation therapy.

ACKNOWLEDGEMENTS

We thank all the members of our laboratory for their help and encouragement. We also thank Dr. T. Kondo (University of Toyama) for various suggestions and instructions, especially regarding the measurement of the amount of intracellular ROS. This study was supported, in part, by Mitsubishi Pharma Corporation (Tokyo, Japan).

REFERENCES

1. Bernhard, W. A. and Close, D. M. (2004) Charged Particle and Photon Interaction with Matter. Eds. Mozunder, A. and Hatano, Y., pp. 431–470, Marcel Dekker Inc.
2. von Sontag, C. (1987) The Chemical Basis of Radiation Biology. Tayler and Fransis, New York.
3. Radford, I. R. and Murphy, T. K. (1994) Radiation response of mouse lymphoid and myeloid cell lines: III. Different signals can lead to apoptosis and may influence sensitivity to killing by DNA double-strand breakage. Int. J. Radiat. Biol. **65**: 229–239.
4. Kerr, J. F. R., Wyllie, A. H. and Currie, A. R. (1972) Apoptosis: a basic biological phenomenon with wide range implications in tissue kinetics. Br. J. Cancer **26**: 239–257.
5. Yamada, T. and Ohyama, H. (1988) Radiation-induced interphase death of rat thymocyte is internally programmed (apoptosis). Int. J. Radiat. Biol. **53**: 65–75.
6. Hosokawa, Y., Tanaka, L., Kaneko, M., Sakakura, Y., Tsuruga, E., Irie, K. and Yajima, T. (2002) Apoptosis induced by generated OH radicals inside cells after irradiation. Arch. Histol. Cytol **65**: 301–305.
7. Watanabe, T., Yuki, S., Egawa, M. and Nishi, H. (1994) Pro-

tective effects of MCI-186 on cerebral ischemia: Possible involvement of free radical scavenging and antioxidant actions. J. Pharmacol. Exp. Ther. **268**: 1597–1603.
8. Yamamoto, T., Yuki, S., Watanabe, T., Mitsuka, M., Saito, K. and Kogure, K. (1997) Delayed neuronal death prevented by inhibition of hydroxyl radical formation in a transient cerebral ischemia. Brain Res. **762**: 240–242.
9. Mizuno, A., Uemura, K. and Nakashima, M. (1998) Inhibitory effect of MCI-186, a free radical scavenger, on cerebral ischemia following rat middle cerebral artery occlusion. Gen. Parmacol. **30**: 575–578.
10. Abe, K., Yuki, S. and Kogure, K. (1988) Strong attenuation of ischemic and postischemic brain edema in rats by a novel free radical scavenger. Stroke **19**: 280–285.
11. Nishi, H., Watanabe, T., Sakurai, H., Yuki, S. and Ishibashi, A. (1989) Effect of MCI-186 on brain edema in rats. Stroke **20**: 1236–1240.
12. Watanabe, T. and Egawa, M. (1994) Effects of an antistroke agent MCI-186 on cerebral arachidonate cascade. J. Pharmacol. Exp. Ther. **271**: 1624–1629.
13. Kawai, H., Nakai, H., Suga, M., Yuki, S., Watanabe, T. and Saito, K. -I. (1997) Effects of a novel free radical scavenger, MCI-186, on ischemic brain damage in the rat distal middle cerebral artery occlusion model. J. Pharmacol. Exp. Ther. **281**: 921–927.
14. Watanabe, K., Watanabe, K., Kuwahara, T. and Yamamoto, Y. (1997) Free radical-induced oxidation products of 3-methyl-1-phenyl-2-pyrazolin-5-one (MCI-186). J. Jpn. Oil Chem. Soc. **46**: 797–801.
15. Amemiya, S., Kamiya, Y., Nito, C., Inaba, Y., Kato, K., Ueda, M., Shimazaki, K. and Katayama, Y. (2005) Anti-apoptotic and neuroprotective effects of edaravone following focal ischemia in rats. Eur. J. Pharmacol. **516**: 125–130.
16. Shichinohe, Y., Kuroda, S., Yasuda, H., Ishikawa, T., Iwai, M., Horiuchi, M. and Iwasaki, Y. (2004) Neuroprotective effects of the free radical scavenger Edaravone (MCI-186) in mice permanent focal brain ischemia. Brain Res. **1029**: 200–206.
17. Nito, C., Kamiya, T., Amemiya, S., Kato, K. and Katayama, Y. (2003) The neuroprotective effect of a free radical scavenger and mild hypothermia following transient focal ischemia in rats. Acta. Neurochir. Suppl. **86**: 199–203.
18. Ikeda, T., Xia, XY., Kaneko, M., Sameshima, H. and Ikenoue, T. (2002) Effect of the free radical scavenger, 3-methyl-1-phenyl-2-pyrazolin-5-one (MCI-186), on hypoxia-ischemia-induced brain injury in neonatal rats. Neurosci. Lett. **329**: 33–36.
19. Noor, JI., Ikeda, T., Ueda, Y. and Ikenoue, T. (2005) A free radical scavenger, edaravone, inhibits lipid peroxidation and the production of nitric oxide in hypoxic-ischemic brain damage of neonatal rats. Am. J. Obstet. Gynecol. **193**: 1703–1708.
20. Nakashima, N., Niwa, M., Iwai, T. and Uematsu, T. (1999) Involvement of free radicals in cerebral vascular reperfusion injury evaluated in a transient focal cerebral ischemia model of rat. Free Radic. Biol. Med. **26**: 722–729.
21. Watanabe, T., Morita, I., Nishi, H. and Murota, S. (1988) Preventive effect of MCI-186 on 15-HPETE induced vascular endothelial cell injury *in vitro*. Prostaglandins Leukot. Essent. Fatty Acids **33**: 81–87.
22. Yamaguchi, T., Ida, T., Kobayashi, T., Hiraga, M., Oishi, K., Uchida, M. K. and Echizen, H. (2004) Alterations of antiproliferative effects of serum obtained from patients with acute cerebral infarction treated with a radical scavenger, edaravone, with or without amlodipine using an *in vitro* cultured basilar artery smooth muscle cells. Yakugaku Zasshi **124**: 25–29.
23. Edaravone Acute Infarction Study Group. (2003) Effect of a novel free radical scavenger, edaravone (MCI-186), on acute brain infarction. Randomized placebo-controlled, double-blind study at multicenters. Cerebrovasc Dis. **15**: 222–229.
24. Toyoda, K., Fujii, K., Kamouchi, M., Nakane, H., Arihiro, S., Okada, Y., Ibayashi, S. and Iida, M. (2004) Free radical scavenger, edaravone, in stroke with internal carotid artery occlusion. J. Neurol. Sci. **221**: 11–17.
25. Watanabe, T., Tanaka, M., Watanabe, K., Takamatsu, Y. and Tobe, A. (2004) Research and development of the free radical scavenger edaravone as a neuroprotectant. Yakugaku Zasshi. **124**: 99–111.
26. Mishina, M., Komaba, Y., Kobayashi, S., Tanaka, N., Kominami, S., Fukuchi, Y., Mizunari, T., Hamamoto, M., Teramoto, A. and Katayama, Y. (2005) Efficacy of edaravone, a free radical scavenger, for the treatment of acute lacunar infarction. Neurol. Med. Chir. (Tokyo) **45**: 344–348. discussion 348.
27. Watanabe, K., Watanabe, K. and Hayase, T. (1997) Radical scavenging mechanism of MCI-186. Jpn. Pharmacol. Ther. **25**: S1699–S1707.
28. Watanabe, K., Watanabe, K., Kuwahara, T. and Yamamoto, Y. (1997) Free radical-induced oxidation products of 3-methyl-1-phenyl-2-pyrazolin-5-one (MCI-186). J. Jpn. Oil. Chem. Soc. **46**: 797–801.
29. Abe, S., Kirima, K., Tsuchiya, K., Okamoto, M., Hasegawa, T., Houchi, H., Yoshizumi, M. and Tamaki, T. (2004) The reaction rate of edaravone (3-methyl-1-phenyl-2-pyrazolin-5-one (MCI-186)) with hydroxyl radical. Chem. Pharm. Bull. **52**: 186–191.
30. Anzai, K., Furuse, M., Yoshida, A., Matsuyama, A., Moritake, T., Tsuboi, K. and Ikota, N. (2003) *In vivo* radioprotection of mice by 3-methyl-1-phenyl-2-pyrazolin-5-one (Edaravone; Radicut), a clinical drug. J. Radiat. Res. **45**: 319–323.
31. Peng, R., Wang, D., Wang, B., Xia, G., Li, Y., Xiong, C., Gao, Y., Yang, H. and Cui, Y. (1999) Apoptosis of hemopoietic cells in irradiated mouse bone marrow. J. Environ. Pathol. Toxicol. Oncol. **18**: 305–308.
32. Nakano, H., Kohara, M. and Shinohara, K. (2001) Evaluation of the relative contribution of p53-mediated pathway in X-ray-induced apoptosis in human leukemic MOLT-4 cells by transfection with a mutant p53 gene at different expression levels. Cell Tissue Res. **306**: 101–106.
33. Morita, A., Suzuki, N., Matsumoto, Y., Hirano, K., Enomoto, A., Zhu, J. and Sakai, K. (2000) p41 as a possible marker for cell death is generated by caspase cleavage of p42/SET β in irradiated MOLT-4 cells. Biochem. Biophys. Res. Commun. **278**: 627–632.
34. Enomoto, A., Suzuki, N., Hirano, K., Matsumoto, Y., Morita, A., Sakai, K. and Koyama, H. (2000) Involvement of SAPK/

JNK pathway in X-ray-induced rapid cell death of human T-cell leukemia cell line MOLT-4. Cancer Lett. **155**: 137–144.
35. Enomoto, A., Suzuki, N., Kang, Y., Hirano, K., Matsumoto, Y., Zhu, J., Morita, A., Hosoi, Y., Sakai, K. and Koyama, H. (2003) Decreased *c*-Myc expression and its involvement in X-ray-induced apoptotic cell death of human T-cell leukemia cell line MOLT-4. Int. J. Radiat. Biol. **79**: 589–600.
36. Nakano, H., Yonekawa, H. and Shinohara, K. (2003) Delayed expression of apoptosis in X-irradiated human leukemic MOLT-4 cells transfected with mutant p53. J. Radiat. Res. (Tokyo) **44**: 179–183.
37. Shinohara, K. and Nakano, H. (1993) Interphase death and reproductive death in X-irradiated MOLT-4 cells. Radiat. Res. **135**: 197–205.
38. Nishikawa, T., Edelstein, D., Du, X. L., Yamagishi, S., Matsumura, T., Kaneda, Y., Yorek, M. A., Beebe, D., Oates, P. J., Hammes, H. P., Giardino, I. and Brownlee, M. (2000) Normalizing mitochondrial superoxide production blocks three pathways of hyperglycaemic damage. Nature. **404**: 787–790.
39. Nagata, S. (2000) Apoptotic DNA fragmentation. Exp. Cell Res. **256**: 12–18.
40. Akagi, Y., Ito, K. and Sawada, S. (1993) Radiation induced apoptosis and necrosis in Molt-4 cells: a study of dose effect relationships and their modification. Int. J. Radiat. Biol. **64**: 47–56.
41. Cui, Z. G., Kondo, T., Feril, Jr. L. B., Waki, K., Inanami, O. and Kuwabara, M. (2004) Effects of antioxidants on X-ray- or hyperthermia- induced apoptosis in human lymphoma U937 cells. Apoptosis **9**: 757–763.
42. Salganik, R. I. (2001) The benefits and hazards of antioxidants: Controlling apoptosis and other protective mechanisms in cancer patients and the human population. J. Am. Coll. Nutr. **20**: 464S–472S.
43. Wahl, G. M. and Carr, A. M. (2001) The evolution of diverse biological responses to DNA damage: insights from yeast and p53. Nature Cell Biol. **3**: E277–E286.
44. Crosby, M. E., Oancea, M. and Almasan, A. (2004) p53 binding to target sites is dynamically regulated before and after ionizing radiation-mediated DNA damage. J. Environ. Pathol. Toxicol. Oncol. **23**: 67–79.
45. Morita, A., Zhu, J., Suzuki, N., Enomoto, A., Matsumoto, Y., Tomita, M., Suzuki, T., Ohtomo, K. and Hosoi, Y. (2006) Sodium orthovanadate suppresses DNA damage-induced caspase activation and apoptosis by inactivating p53. Cell Death Differ. **341**: 499–511.
46. Zheng, T. S., Hunot, S., Kuida, K. and Flavell, R. A. (1999) Caspase knockouts: matters of life and death. Cell Death Differ. **6**: 402–411.
47. Nicholson, D. W. (1999) Caspase structure, proteolytic substrates, and function during apoptotic cell death. Cell Death Differ. **6**: 1028–1042.
48. Gross, A., McDonnell, J. M. and Korsmeyer, S. J. (1999) BCL-2 family members and the mitochondria in apoptosis. Genes. Dev. **13**: 1899–1911.
49. Cheng, E. H., Kirsch, D. G., Clem, R. J., Ravi, R., Kastan, M. B., Bedi, A., Ueno, K. and Hardwick, J. M. (1997) Conversion of Bcl-2 to a Bax-like death effector by caspases. Science **278**: 1966–1968.
50. Rajesh, K. G., Sasaguri, S., Suzuki, R. and Maeda, H. (2003) Antioxidant MCI-186 inhibits mitochondrial permeability transition pore and upregulates Bcl-2 expression. Am. J. Physiol. Heart Circ. Physiol. **285**: H2171–H2178.
51. Song, Y., Li, M., Li, J. C. and Wei, E. Q. (2006) Edaravone protects PC12 cells from ischemic like injury via attenuating the damage to mitochondria. J. Zhejiang Univ. Sci. B **7**: 749–756.
52. Mantovani, G., Maccio, A., Madeddu, C., Mura, L., Gramignano, G., Russo, M. R., Murgia, V., Camboni, P., Ferreli, L., Mocci, M. and Massa, E. (2003) The impact of different antioxidant agents alone or in combination on reactive oxygen species, antioxidant enzymes and cytokines in a series of advanced cancer patients at different sites: correlation with disease progression. Free Radic. Res. **37**: 213–223.
53. McClain, D. E., Kalinich, J. F. and Ramakrishnan, N. (1995) Trolox inhibits apoptosis in irradiated MOLT-4 lymphocytes. FASEB J. **9**: 1345–1354.
54. Inanami, O., Takahashi, K. and Kuwabara, M. (1999) Attenuation of caspase-3-dependent apoptosis by Trolox post-treatment of X-irradiated MOLT-4 cells. Int. J. Radiat. Biol. **75**: 155–163.
55. Zhang, N., Komine-Kobayashi, M., Tanaka, R., Liu, M., Mizuno, Y. and Urabe, T. (2005) Edaravone reduces early accumulation of oxidative products and sequential inflammatory responses after transient focal ischemia in mice brain. Stroke. **36**: 2220–2225.
56. Yagi, Y., Horinaka, S. and Matsuoka, H. (2005) Edaravone prevented deteriorated cardiac function after myocardial ischemia-reperfusion via inhibiting lipid peroxidation in rat. J. Cardiovasc. Pharmacol. **46**: 46–51.
57. Marzatico, F., Porta, C., Moroni, M., Bertorelli, L., Borasio, E., Finotti, N., Pansarasa, O. and Castagna, L. (2000) *In vitro* antioxidant properties of amifostine (WR-2721, Ethyol). Cancer Chemother. Pharmacol. **45**: 172–176.
58. Grdina, D. J., Kataoka, Y., Basic, I. and Perrin, J. (1992) The radioprotector WR-2721 reduces neutron-induced mutations at the hypoxanthine-guanine phosphoribosyl transferase locus in mouse splenocytes when administered prior to or following irradiation. Carcinogenesis **13**: 811–814.

Received on May 24, 2007
Revision received on July 5, 2007
Accepted on August 3, 2007
J-STAGE Advance Publication Date: October 24, 2007

ELSEVIER

Int. J. Radiation Oncology Biol. Phys., Vol. 69, No. 4, pp. 970–973, 2007

0360-3016/07/$–see front matter

doi:10.1016/j.ijrobp.2007.08.026

RAPID COMMUNICATION

VERIFICATION OF IN-TREATMENT TUMOR POSITION USING KILOVOLTAGE CONE-BEAM COMPUTED TOMOGRAPHY: A PRELIMINARY STUDY

KEIICHI NAKAGAWA, M.D., PH.D.,* HIDEOMI YAMASHITA, M.D., PH.D.,* KENSHIRO SHIRAISHI, M.D., PH.D.,* HIROSHI IGAKI, M.D., PH.D.,* ATSURO TERAHARA, M.D., PH.D.,* NAOKI NAKAMURA, M.D.,* KUNI OHTOMO, M.D., PH.D.,* SHIGEKI SAEGUSA, R.T.T.,* TAKASHI SHIRAKI, R.T.T.,* TAKASHI ORITATE, R.T.T.,* AND KIYOSHI YODA, PH.D.†

*Department of Radiology, University of Tokyo Hospital, Tokyo, Japan; and †Elekta, KK, Kobe, Japan

Three-dimensional tumor position during rotational dose delivery was evaluated by acquiring in-treatment kilovoltage (kV) cone-beam CT (CBCT) to ensure treatment quality. The CBCT projection data of a phantom were acquired during rotational megavoltage (MV) dose delivery up to 6 Gy to evaluate image quality under MV beam irradiation. A lung tumor patient was treated with a total dose of 48 Gy in four fractions, each fraction including seven coplanar and noncoplanar beams, as well as a full-angle rotational beam. Tumor registration was performed between a planning CT image and a CBCT image immediately after patient setup. The patient couch was adjusted according to the registration results, and then the registration was repeated three times: immediately before treatment, during treatment, and immediately after treatment. The phantom image quality of the kV CBCT was not visually degraded up to the rotational MV dose of 6 Gy. Tumor position during rotational dose delivery was verified for the first time using kV CBCT. © 2007 Elsevier Inc.

SRT, Cone-beam CT, Rotational therapy, Quality assurance.

INTRODUCTION

The purpose of image-guided radiotherapy is to localize a tumor at the predetermined position of treatment planning, and the quality of image-guided radiotherapy can be accurately verified by monitoring tumor position during dose delivery. Previous methods for detecting a tumor position during dose delivery include fluoroscopic marker detection (1), electromagnetic coil localization (2), and ultrasound tumor monitoring (3). Fluoroscopic marker detection and electromagnetic coil localization require surgery to embed the marker or the coil on the surface of tumor. In addition, a number of inserts are required to extract tumor orientation information, which is not always easy to accomplish. Ultrasound imaging is a noninvasive approach, but it is not easily applicable to a lung tumor because of air in the lung, which causes significant ultrasound signal attenuation.

Tumor registration using cone-beam computed tomography (CBCT) has been verified either immediately before or after beam delivery (4), and it was assumed that the tumor position remains unchanged during treatment.

The purpose of this article is to report for the first time that CBCT-based direct verification during beam delivery is feasible.

METHODS AND MATERIALS

Phantom study

Using Elekta Synergy (Elekta, Crawly, United Kingdom), kilovoltage (kV) CBCT projection data of a phantom were acquired during rotational megavoltage (MV) dose delivery up to 6 Gy to evaluate CBCT image quality under MV beam irradiation. The Synergy system with X-ray volume imaging functionality (XVI 4.0) did not allow simultaneous kV CBCT beams and rotational MV beams; therefore, a method for disabling this interlock was investigated, and it was deactivated with the first author's responsibility. Throughout this investigation, the photon energy was 6 MV and Pinnacle (ADAC Laboratories, Milipitas, CA) was used for treatment planning. The data acquisition time for CBCT was always 2 min for a full gantry rotation.

Patient study

A lung tumor patient was treated in four fractions, each with 12 Gy. Each fraction included seven coplanar and noncoplanar

Reprint requests to: Keiichi Nakagawa, M.D., Ph.D., Department of Radiology, University of Tokyo Hospital, 7-3-1 Hongo Bunkyo-Ku, Tokyo 113-8655, Japan; E-mail: k-nak@fg7.so-net.ne.jp

Conflict of interest: Dr. Nakagawa receives research funding from Elekta K.K.

Received July 25, 2007, and in revised form Aug 2, 2007. Accepted for publication Aug 2, 2007.

beams, as well as a full-angle rotational beam. Each field of the seven static beams was defined by multileaf collimators and that of the rotational beam was done by static x and y jaws. The Elekta Stereotactic Body Frame (SBF) was also used to minimize breathing artifact both for treatment planning CT and CBCT imaging. Using built-in software, bone-matching registration was performed between the treatment-planning CT image and a CBCT image immediately after patient setup. The patient couch was adjusted according to the registration results, and then the registration was repeated by taking another CBCT image. During the rotational beam delivery, more kV CBCT image data were acquired to verify the tumor position. Still more kV CBCT image data were acquired immediately after treatment.

RESULTS

Phantom study

Figure 1 shows kV CBCT coronal images of a lung phantom during MV rotational dose delivery with a field size of 10 × 10 cm^2, where (a) corresponds to 0 Gy and (b) corresponds to 6 Gy. No additional noise was observed when 6 Gy was delivered to the phantom. Crossed lines indicate the isocenter.

Patient study

Figure 2 shows overlaid coronal images of the planning CT and CBCT before and after registration. Although transverse and sagittal images are not shown here, the registration was performed in three dimensions, and the dotted lines indicate boundaries of the volume of interest, within which a bone-matching technique was applied.

Figure 3 demonstrates kV CBCT coronal images of a lung tumor patient before registration (Fig. 3a), immediately before treatment and after registration (Fig. 3b), during treatment (Fig. 3c), and immediately after treatment (Fig. 3d). Again, the crossed lines indicate the isocenter.

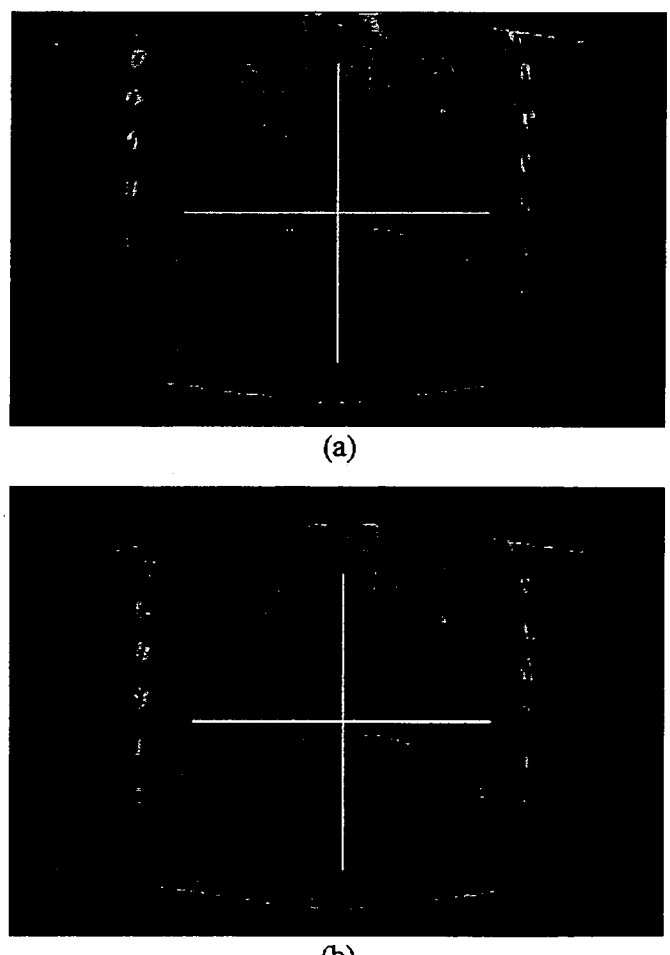

Fig. 1. Kilovoltage cone-beam computed tomography (CT) coronal images of lung phantom during megavoltage rotational dose delivery with a field size of 10 × 10 cm^2. (a) 0 Gy. (b) 6 Gy. No additional noise was observed when 6 Gy was delivered to the phantom. Crossed lines indicate the isocenter.

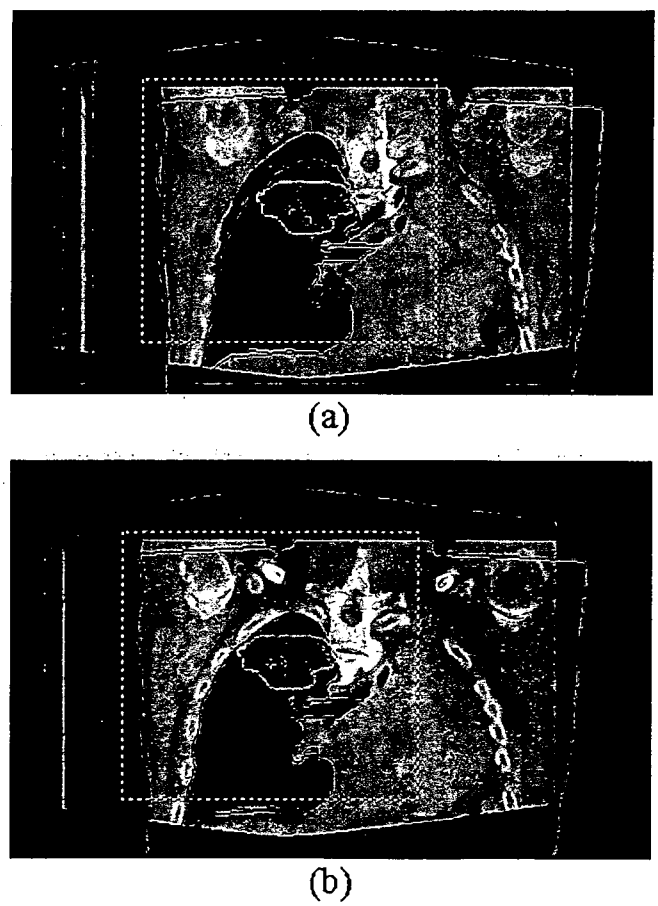

Fig. 2. Overlaid coronal images of the planning computed tomography (CT) and cone-beam CT (a) before and (b) after registration. Although transverse and sagittal images are not shown here, the registration was performed in three dimensions, and the dotted lines indicate boundaries of the volume of interest, within which a bone-matching technique was applied.

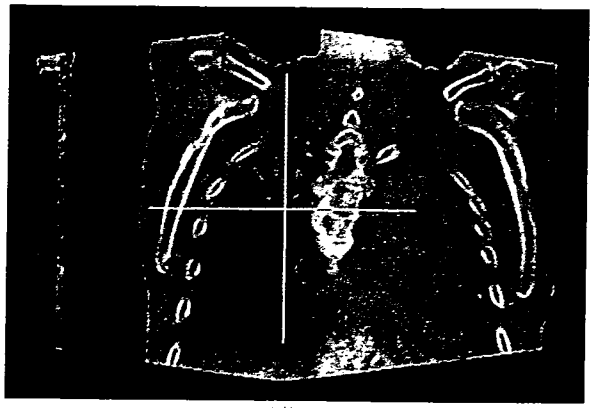

(a)

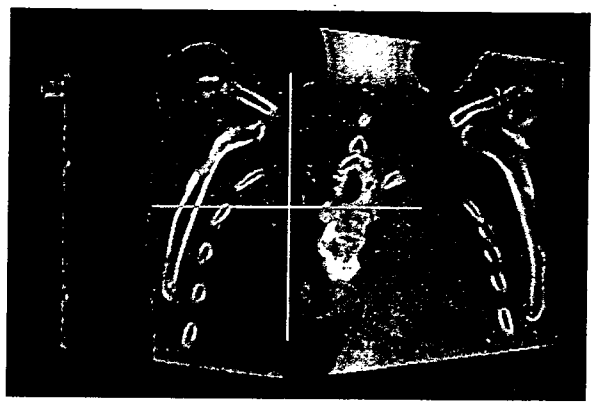

(b)

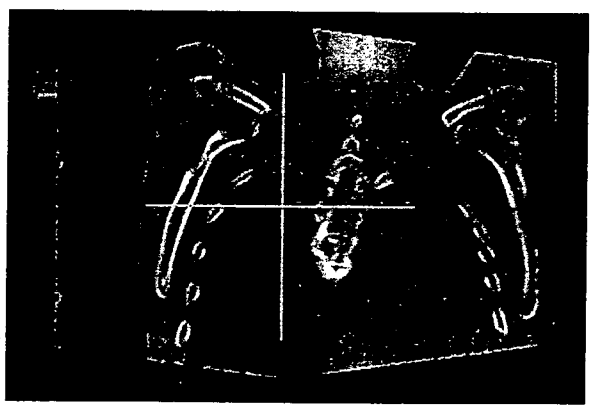

(c)

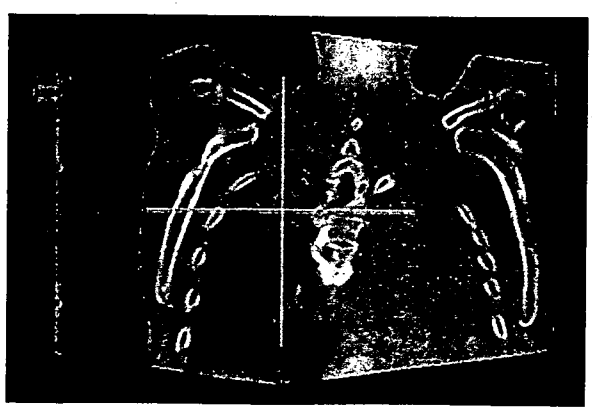

(d)

Fig. 3. Kilovoltage cone-beam computed tomography coronal images of a lung tumor patient (a) before registration, (b) immediately before treatment and after registration, (c) during treatment, and (d) immediately after treatment. Crossed lines indicate the isocenter.

Table 1 provides calculated registration errors between the planning CT image and each of the CBCT images acquired at the above four different times. The registration was performed for each fraction using a built-in bone-matching procedure.

DISCUSSION

Figure 1 indicates that MV treatment beams do not practically degrade projection images for kV CBCT reconstruction. In a previous real-time fluoroscopic system, a blanking control was required to reduce the background level of kV image detectors (5). A major difference is the angle between the MV port and the kV port; in other words, the angle is 90° in Synergy and nearly 45° in the previous fluoroscopic system. It is anticipated that the orthogonal design minimized noise contamination to the kV detector of Synergy.

Initially we thought that the Elekta SBF was not required for patient setup because of Synergy's CBCT functionality. However, it was found that the breathing artifact of lung CBCT images was significantly reduced by using the SBF. After this was recognized, all the planning CT images and Synergy CBCT images were taken with the SBF.

The reconstructed isotropic voxel size of the CBCT volume image was 1 mm, and the planning CT slice width was also 1 mm; therefore, the registration error of <1 mm shown in Table 1 was within measurement precision. This indicates that there are no significant differences in registration errors among pretreatment, in-treatment, and posttreatment CBCT images of the treated patient. At the time of writing, 12 patients have received radiotherapy including rotational treatment with simultaneous CBCT imaging. Of 12 patients, 8 had lung tumors, 3 had liver cancers, and 1 had a brain tumor.

In this report we only verified the patient tumor position among one of the eight beams, which was a full-angle rotational beam with constant x and y jaw positions. This was because at present the Synergy linear accelerator controller does not allow dynamic arc dose delivery. It is anticipated that dynamic treatment will be supported in the near future, and the present technique will be best performed with dynamic arc treatment including intensity-modulated arc therapy (6) as well as conventional rotational conformal therapy. Last, in-treatment registration information may be useful in subsequent treatment margin or dose adjustment.

Table 1. Calculated registration error between planning CT image and each CBCT image acquired before registration, before treatment, during treatment, and immediately after treatment

Date*	Time†	CBCT timing	Lateral (mm)	Longitudinal (mm)	Vertical (mm)
20070305	170458	Before registration	−1.0	19.7	−0.8
	171306	Before treatment	0.5	−0.7	−1.0
	173411	During treatment	0.9	−0.9	−1.3
	173925	After treatment	1.1	−0.6	−1.3
20070306	154453	Before registration	0.6	21.3	1.3
	155105	Before treatment	0.2	−0.3	−0.3
	160905	During treatment	0.2	−0.7	−0.9
	161531	After treatment	0.2	−0.1	−1.5
20070307	163829	Before registration	1.9	15.8	−0.5
	164751	Before treatment	0.3	0.4	0.8
	171012	During treatment	0.2	−0.3	1.4
	171613	After treatment	−0.4	−0.1	1.3
20070308	165155	Before registration	0.7	23.0	0.4
	165949	Before treatment	0.3	−0.1	−0.4
	171916	During treatment	0.4	−0.4	−0.4
	172419	After treatment	0.2	−0.2	−0.6

Abbreviations: CT = computed tomography; CBCT = cone-beam CT.
Registration was performed for each fraction using a built-in bone-matching procedure.
* Date is listed as year/month/day (yyyymmdd).
† Time is listed as hour/minute/sec (hhmmss).

REFERENCES

1. Shirato H, Shimizu S, Shimizu T, *et al.* Real-time tumour-tracking radiotherapy. *Lancet* 1999;353:1331–1332.
2. Seiler PG, Blattmann H, Kirsch S, *et al.* A novel tracking technique for the continuous precise measurement of tumour positions in conformal radiotherapy. *Phys Med Biol* 2000;45:N103–N110.
3. Sawada A, Yoda K, Kokubo M, *et al.* A technique for noninvasive respiratory gated radiation treatment system based on a real time 3D ultrasound image correlation: A phantom study. *Med Phys* 2004;31:245–250.
4. Jaffray DA, Siewerdsen JH, Wong JW, *et al.* Flat-panel cone-beam computed tomography for image-guided radiation therapy. *Int J Radiat Oncol Biol Phys* 2002;53:1337–1349.
5. Shirato H, Shimizu S, Kunieda T, *et al.* Physical aspects of a real-time tumor-tracking system for gated radiotherapy. *Int J Radiat Oncol Biol Phys* 2000;48:1187–1195.
6. Yu CX. Intensity-modulated arc therapy with dynamic multileaf collimation: An alternative to tomotherapy. *Phys Med Biol* 1995; 40:1435–1449.